Supporting information

Experimental setup

To measure the microwave photoconductivity signal of a sample, a custom-built setup similar to that described by Asada et al.[23] is used. The sample is placed in front of a microwave waveguide with dimensions 22.86 x 10.16mm through which it is irradiated with continuous microwave radiation. Figure SI 1 offers a schematic representation of the working principle and an image depicting the setup and its components can be found in Figure SI 2. Excitation can be switched between two lasers with 532nm (*CryLas*, eMOPA532-200-E-STA) and 355nm (*CryLas*, eMOPA355-100-E-OEM) wavelength respectively, though only the 532nm laser was used in this study. The beam path of the 355nm laser is merged with that of the 532 nm laser by a combination of a regular mirror and a dichroic mirror (*Thorlabs*, HBSY13) which transmits the 532nm light and reflects the 355nm light. Both lasers are operated in pulsed mode with a repetition frequency of 1kHz. A filter holder allows for attenuation of the light intensity through filters with varying optical density. A lens is used to expand the laser beam and an iris aperture restricts the illuminated area to a circular region of 2.4cm². This reduces the irradiance on the sample and prevents damage. Furthermore, since the microwave field extends over the whole waveguide area with constant intensity along the short dimension and a Gaussian intensity distribution along the long axis, this setup improves the signal by illuminating a larger fraction of the sample, which contributes to the overall signal.

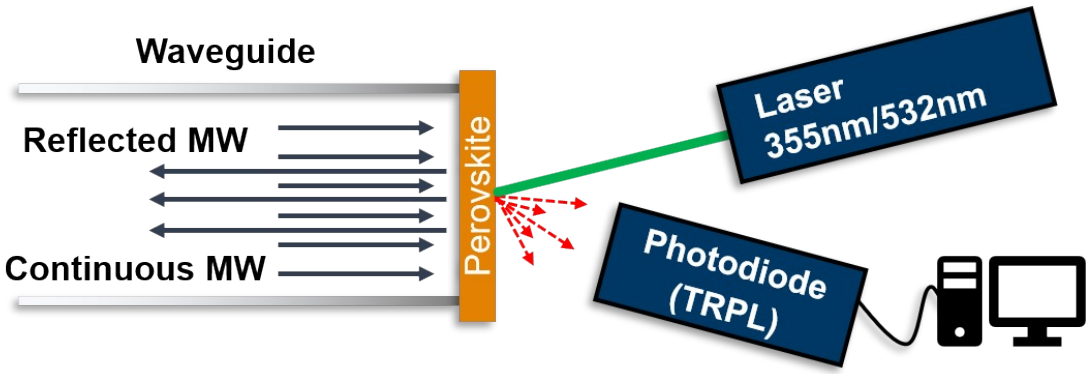

Figure SI 1: Schematic representation of the working principle of microwave photoconductivity measurements. Continuous microwave radiation is directed at a sample and the transient reflected power is measured. Upon excitation with a pulsed laser, the additionally created charge carriers change the reflection behaviour. Additionally, a fast photodiode can be implemented to simultaneously capture trPL.

The required microwave radiation is generated by a Gunn-diode, operated at 9V, which produces continuous microwave radiation in the X-band (9GHz). The microwaves are directed to a circulator which guides the incoming microwaves from the first of its three ports to the next and serves to separate the incident and reflected microwaves. A manual E-H-tuner (*hp*, X880 A) is then employed to optimize the signal by adjusting the resonance condition within the waveguide system. Finally, a bent waveguide with an open end is used as an aperture where the sample can be placed. The microwaves reflected at the sample pass through the E-H-tuner again and are directed to the detector via the circulator, where they are converted into an electrical signal, amplified by an amplifier (*FEMTO*, HVA-200M-40-F), and recorded by an oscilloscope with a time-resolution of 2.5GS/s (*Tektronix*, DPO3034). It is important to note that the laser is incident on the opposite side of the sample compared to the microwaves. Samples are usually deposited on a glass substrate, with the glass side fixed on the waveguide opening, though other sample types, such as powders or pellets, can also be measured.

In addition to the microwave components, a fast photodiode (*Hamamatsu*, S5972) positioned beside the sample is employed to capture trPL signals. This photodiode is equipped with a 375nm long pass filter (*Schott*) and a 532nm step-filter (*Thorlabs*) to remove both of the exciting laser wavelengths. The trPL signal is recorded via a second channel of the same oscilloscope.

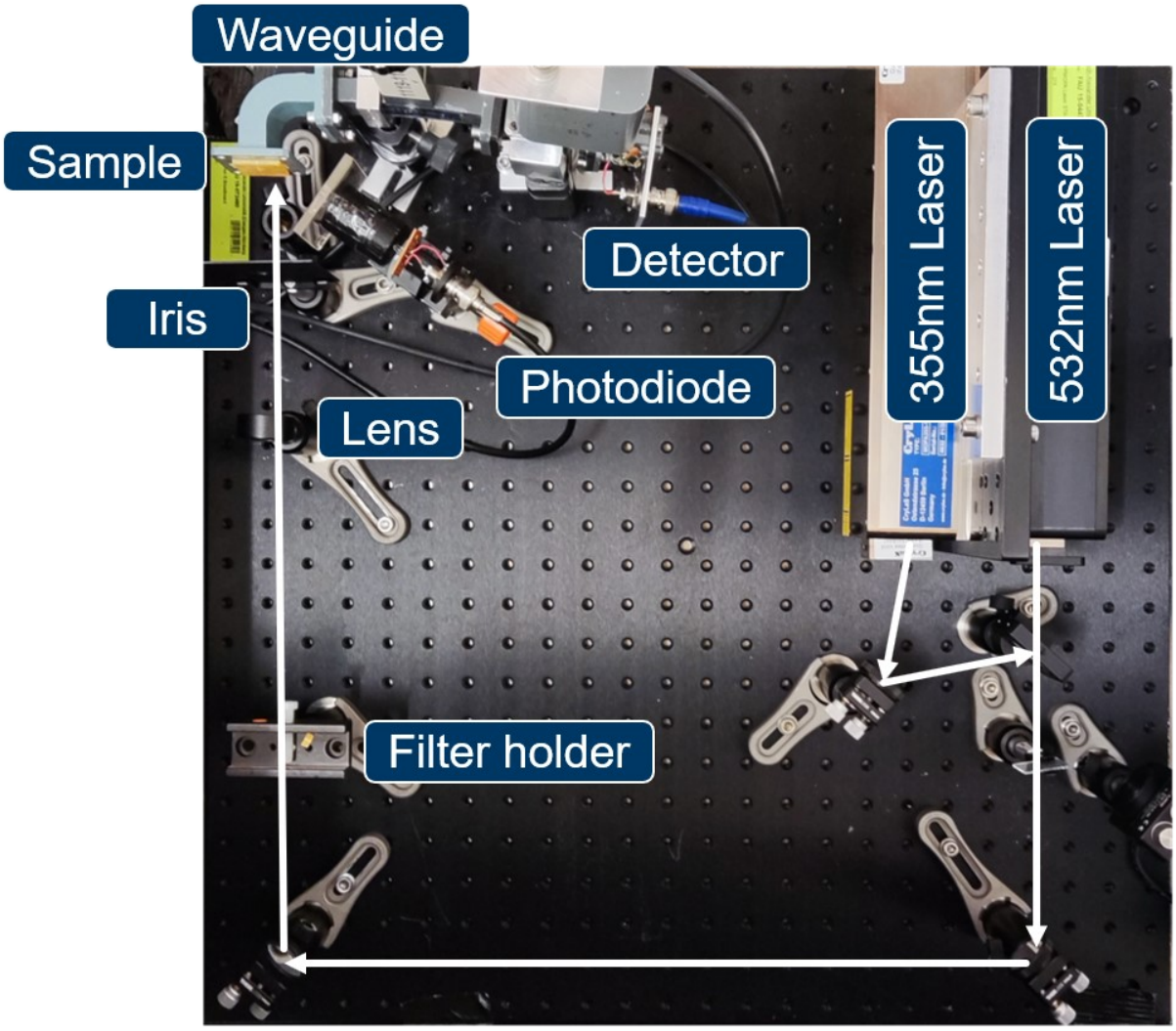

Figure SI 2: Image of the measurement setup annotated with the used components. The white arrows indicate the beam path of the lasers.

Experimental details

Sample fabrication

The samples investigated in this study are thin films of triple-cation, mixed-halide perovskite with a stoichiometric composition of $FA_{0.82}MA_{0.13}Cs_{0.05}Pb(I_{0.87}Br_{0.13})_3$. These films were deposited on glass substrates via spin coating from a precursor solution with a concentration of 1.5M. A passivating layer of PEAI/MAI (2:1, wt./wt.), which was dissolved in IPA-DMF (200:1, v/v), was then applied by spin coating at 4000RPM for 30 seconds. Subsequently, the samples were annealed for 20 minutes at either 25°C, 60°C or 100°C in an inert nitrogen atmosphere and in a vacuum chamber at room temperature respectively.

Measurement conduct

The samples were kept in inert atmosphere until shortly before the measurement. They were mounted on the open end of the waveguide and measured as described. Both time-resolved photoluminescence and microwave photoconductivity signals were recorded simultaneously, using a fast oscilloscope and saved on a computer. Intensity-dependent measurements were performed by inserting a neutral density step filter (*Thorlabs*, NDL-25S-2) into the laser beam path.

The measurements were exclusively performed using a 532nm laser and the pulse energy was determined to be 62µJ with a pyroelectric power meter. Considering the laser spot area of 2.4cm² and the single photon energy at 532nm of 3.7×10^{-19}J, the number of photons per pulse and area was calculated to be $6.9\times10^{17}m^{-2}$. Assuming a layer thickness of 650nm and an absorption coefficient equivalent to that of pure $MAPbI_3$ ($\alpha = 6087100\ m^{-1}$), it was calculated that over 98% of the light was absorbed. Furthermore, it was assumed that charge carrier diffusion laterally through the layer is much faster than any recombination processes leading to an average charge carrier density of $1.0E+24m^{-3}$ after diffusion. The same procedure was employed for lower intensity conditions, where the laser power was attenuated by an optical filter.

Data treatment and fitting

Before performing the analysis, the recorded trPL and microwave photoconductivity data needed to be treated. Firstly, the signal background was determined by calculating the mean of the data before the rise of the signal. Additionally, we determined the noise level by calculating the standard deviation of data points in the same time range. Subsequently, the background was subtracted from the signal and the signal was truncated and shifted such that the photoluminescence signal peaked at time t=0. Furthermore, the signal was multiplied by the sign of the peak value to ensure a positive peak for the analysis.

Since the measurement data consists of a large number of datapoints, the data was re-interpolated to 1000 evenly spaced points. Due to the large parameter range of multiple orders of magnitude, the logarithm of the data was calculated and used for the further steps. This improves the optimization and ensures that the algorithm works consistently over a large range of parameter values. However, this presented a problem with zero and negative values in the signal data, which were therefore removed from the analysis.

The fact that the simulated signal could approach zero also needed to be considered since this is not representative of the experimentally measured signal due to limited detector resolution and noise. This consequently caused the experimental and simulated trPL signals to diverge after a certain point. To address this issue, we assumed that the signal noise is normally distributed with a mean value of 0 after subtracting the background. Since values below 0 were removed during the conversion to logarithmic scaling, the average of the half-Gaussian distribution provides the correct background for the signal. For an initially Gaussian distribution with width σ, this background b is then given by: $b = \sigma\sqrt{\frac{2}{\pi}}$, where σ is the previously calculated noise level. This background was then added as a constant term to the simulated signal as a baseline.

The fitting algorithm was then employed to optimize the values of the parameters $k_B, k_T, k_D, r_\mu, N_T, I_{PL}$ and I_{MW}. Notably, the doping density p_0 was not optimized but instead fixed at

zero since there was no deliberate effort to produce doped samples. While perovskites may exhibit self-doping,[22] it was assumed that the resulting doping density from this effect is negligible.

Bayesian optimization for automatic research (BOAR)

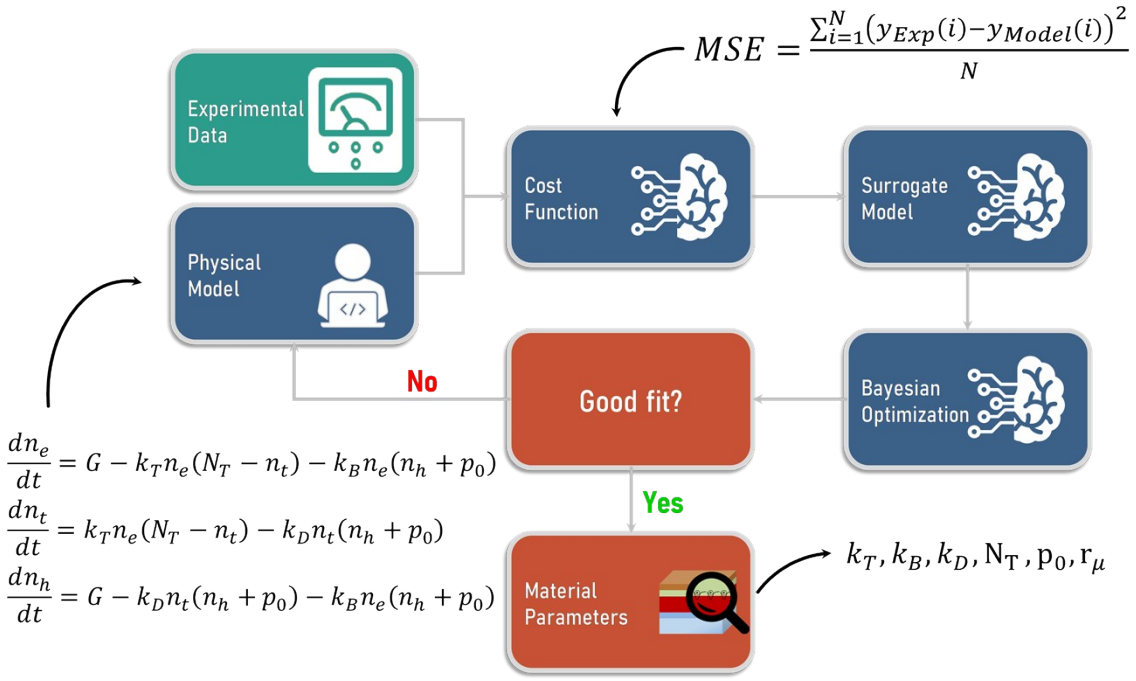

Figure SI 3: Schematic workflow of BOAR (Bayesian optimization for automatic research).

Fitting of synthetic data

Simulated condition	$k_B\left[\frac{m^3}{s}\right]$	$k_T\left[\frac{m^3}{s}\right]$	$k_D\left[\frac{m^3}{s}\right]$	r_μ	$N_T\left[\frac{1}{m^3}\right]$	$I_{PL}[a.u.]$	$I_{MW}[a.u.]$	$k_T N_T\left[\frac{1}{s}\right]$
25°C-like	2.5×10^{-17}	5.4×10^{-18}	1.75×10^{-18}	4.7	1.3×10^{23}	8.7×10^{-33}	1.4×10^{-26}	7.02×10^{5}
100°C-like	1.8×10^{-17}	9×10^{-18}	7×10^{-17}	2	1.2×10^{23}	8.4×10^{-33}	4.4×10^{-26}	1.08×10^{6}

Table SI 1: Fundamental parameters for the synthetic data.

The synthetic signals were modified by a Gaussian noise term of the form $g(x) = \exp\left(-\frac{(x-x_c)^2}{2\sigma^2}\right)$, where x_c is the centre of the distribution and σ is the width to simulate the noise and background found in real measurements. The parameter values can be found in Table SI 2.

Background PL $x_{c,PL}$	**Standard Dev. PL** σ_{PL}	**Background MW** $x_{c,MW}$	**Standard Dev. MW** σ_{MW}
-3.6×10^{-3}	3.0×10^{-5}	-7.0×10^{-4}	3.8×10^{-5}

Table SI 2: Noise and background used for the production of synthetic data.

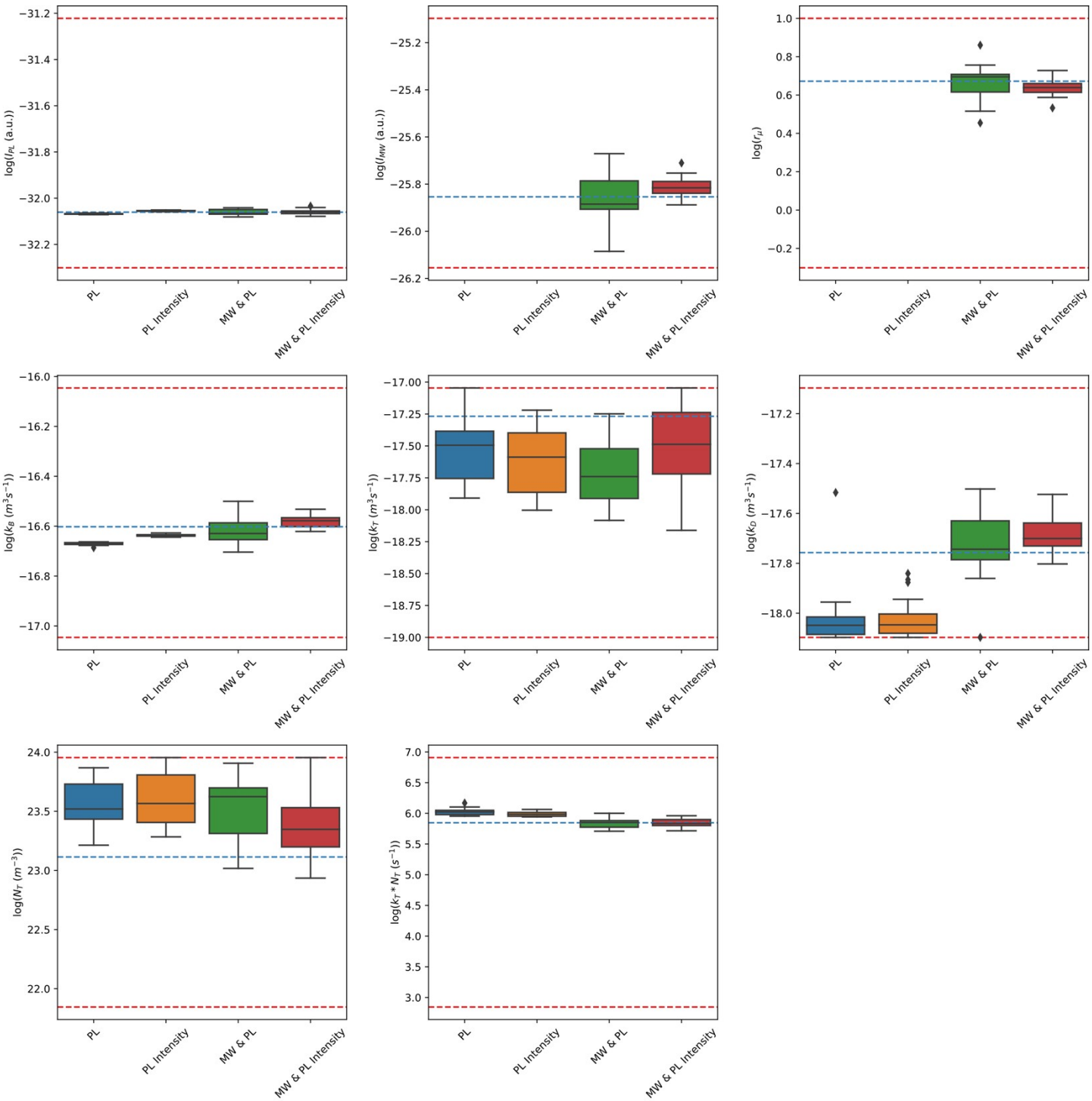

Figure SI 4: Results from 20 iterations of fitting 25°C-like synthetic data. Red dashed lines indicate the range in which each parameter was allowed to vary and blue dashed lines indicate the true value used to produce the synthetic data.

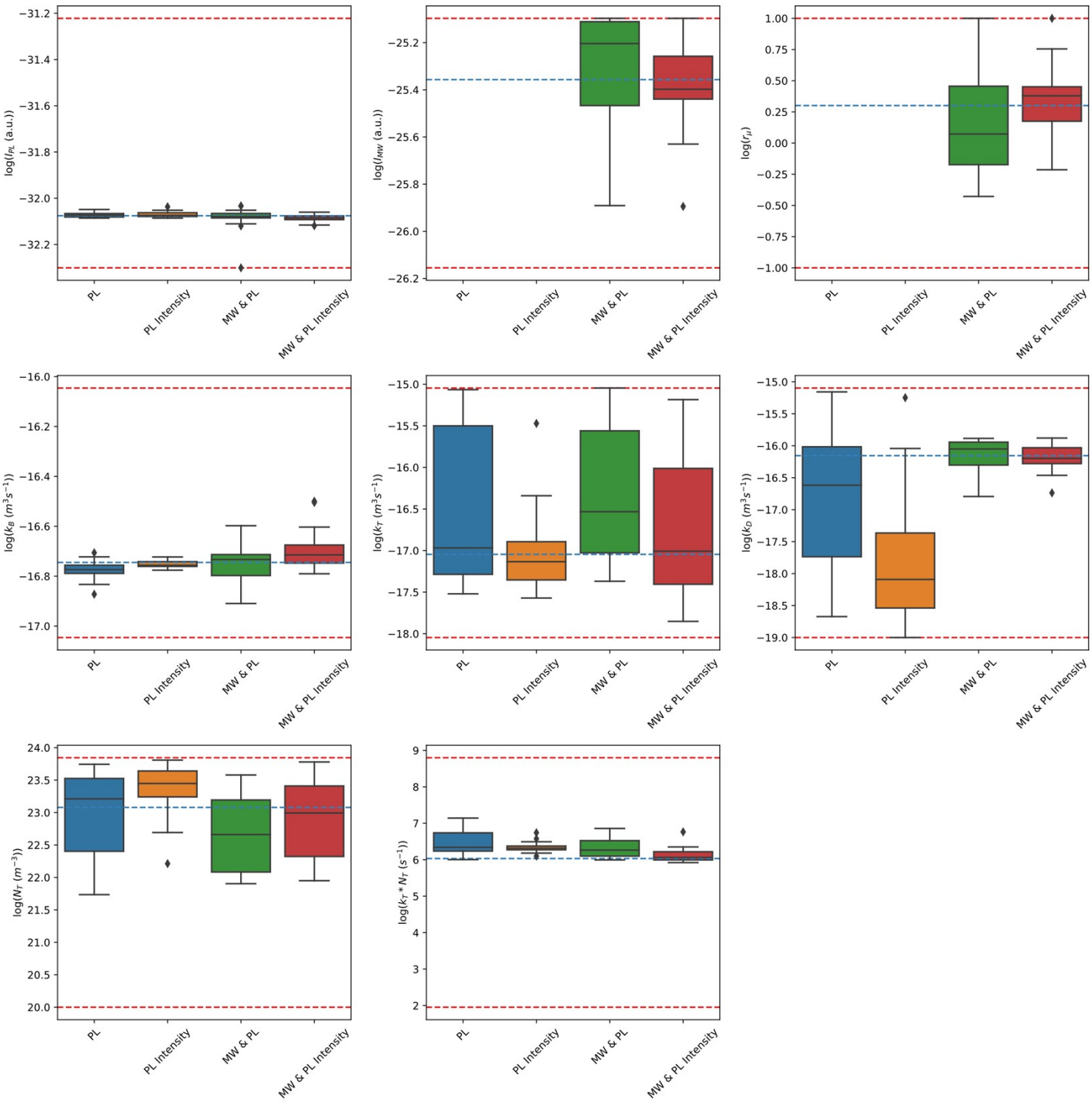

Figure SI 5: Results from 20 iterations of fitting 100°C-like synthetic data. Red dashed lines indicate the range in which each parameter was allowed to vary and blue dashed lines indicate the true value used to produce the synthetic data.

Results

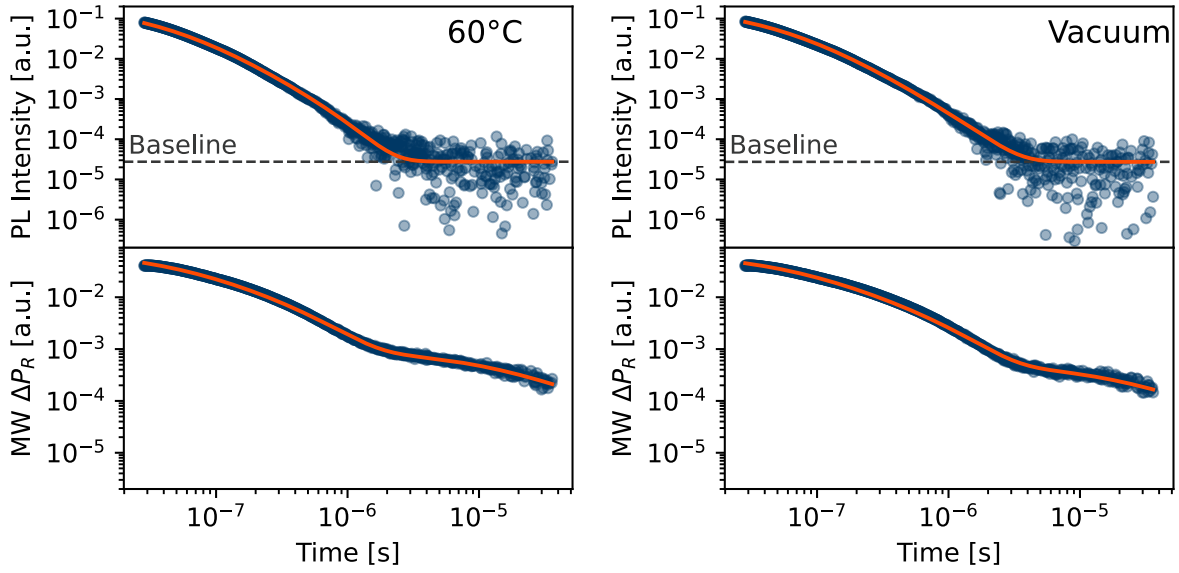

Figure SI 6: Experimental (blue dots) microwave photoconductivity (bottom) and time-resolved photoluminescence (top) data of $FA_{0.82}MA_{0.13}Cs_{0.05}Pb(I_{0.87}Br_{0.13})_3$ annealed for 20 min at 60°C and in vacuum at room temperature respectively. The orange lines are global fits of both trPL and microwave photoconductivity data, produced with BOAR. The dashed grey lines indicate the baselines of the photoluminescence signal.

Parameters extracted from fits

Single-intensity	$k_B\left[\frac{m^3}{s}\right]$	$k_T\left[\frac{m^3}{s}\right]$	$k_D\left[\frac{m^3}{s}\right]$	r_μ	$N_T\left[\frac{1}{m^3}\right]$	$I_{PL}[a.u.]$	$I_{MW}[a.u.]$	$k_T N_T\left[\frac{1}{s}\right]$
Vacuum	1.77×10^{-17}	4.42×10^{-19}	1.20×10^{-18}	5.328	6.89×10^{23}	1.01×10^{-32}	1.05×10^{-26}	3.0×10^{5}
25°C	2.54×10^{-17}	5.43×10^{-18}	1.75×10^{-18}	4.699	1.31×10^{23}	8.71×10^{-33}	1.40×10^{-26}	6.1×10^{5}
60°C	2.21×10^{-17}	1.14×10^{-18}	1.34×10^{-18}	4.629	5.55×10^{23}	8.96×10^{-33}	1.32×10^{-26}	6.3×10^{5}
100°C	1.85×10^{-17}	8.94×10^{-18}	6.95×10^{-17}	0.3392	1.26×10^{23}	8.42×10^{-33}	4.41×10^{-26}	1.1×10^{6}
Intensity-dependent	$k_B\left[\frac{m^3}{s}\right]$	$k_T\left[\frac{m^3}{s}\right]$	$k_D\left[\frac{m^3}{s}\right]$	r_μ	$N_T\left[\frac{1}{m^3}\right]$	$I_{PL}[a.u.]$	$I_{MW}[a.u.]$	$k_T N_T\left[\frac{1}{s}\right]$
Vacuum	2.50×10^{-17}	1.26×10^{-18}	9.34×10^{-19}	7.912	3.02×10^{23}	1.19×10^{-32}	1.15×10^{-26}	3.81×10^{5}
25°C	4.19×10^{-17}	1.77×10^{-18}	3.58×10^{-18}	3.728	2.99×10^{23}	1.01×10^{-32}	2.63×10^{-26}	5.30×10^{5}
60°C	3.82×10^{-17}	4.20×10^{-18}	2.24×10^{-18}	4.404	1.66×10^{23}	1.05×10^{-32}	2.17×10^{-26}	6.98×10^{5}
100°C	3.58×10^{-17}	1.12×10^{-18}	4.07×10^{-17}	2.781	5.16×10^{23}	9.55×10^{-33}	2.82×10^{-26}	5.76×10^{5}

Table SI 3: Summary of all parameters extracted from fitting combined trPL and microwave photoconductivity data with BOAR for both single-intensity and intensity-dependent measurements.

J-V-Curves

J-V-Curves were measured on devices with a Ag/PCBM/PEAI/Perovskite/SAM/NiO_x/ITO structure treated with 100°C thermal annealing and vacuum annealing respectively. The results can be found in Figure SI 7.

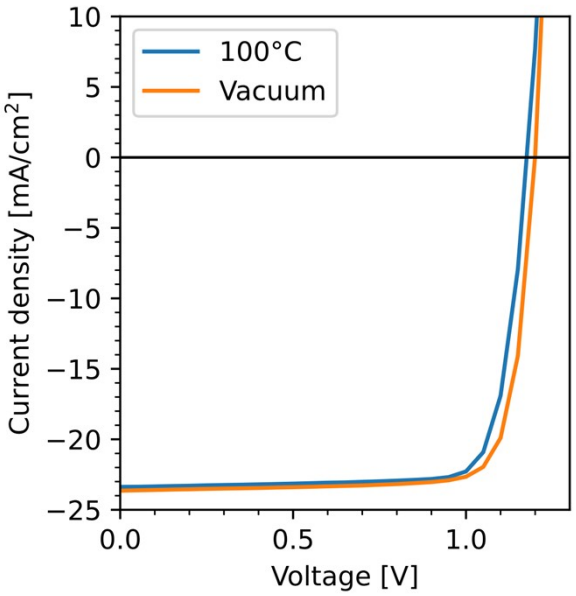

Figure SI 7: Comparison of JV-curves of two devices treated with 100°C thermal annealing and vacuum annealing respectively.